

PandaX-xT – a Multi-ten-tonne Liquid Xenon Observatory at the China Jinping Underground Laboratory

Abdusalam Abdukerim², Zihao Bo², Wei Chen², Xun Chen^{2,3}, Chen Cheng⁴, Zhaokan Cheng⁵, Xiangyi Cui¹, Yingjie Fan⁶, Deqing Fang⁷, Lisheng Geng^{8,9,10,11}, Karl Giboni², Linhui Gu², Xunan Guo⁸, Xuyuan Guo¹², Zhichao Guo⁸, Chencheng Han¹, Ke Han², Changda He², Jinrong He¹⁰, Di Huang², Junting Huang², Zhou Huang², Ruquan Hou³, Yu Hou¹³, Xiangdong Ji¹⁴, Yonglin Ju¹³, Chenxiang Li², Jiafu Li⁴, Mingchuan Li¹², Shuaijie Li^{12,1}, Tao Li⁵, Qing Lin^{15,16}, Jianglai Liu^{*1,2,3}, Congcong Lu¹³, Xiaoying Lu^{17,18}, Lingyin Luo¹⁹, Yunyang Luo¹⁶, Wenbo Ma², Yugang Ma⁷, Yajun Mao¹⁹, Yue Meng^{2,3}, Xuyang Ning², Binyu Pang^{17,18}, Ningchun Qi¹², Zhicheng Qian², Xiangxiang Ren^{17,18}, Nasir Shaheed^{17,18}, Xiaofeng Shang², Xiyuan Shao²⁰, Guofang Shen⁸, Lin Si², Wenliang Sun¹², Yi Tao^{2,3}, Anqing Wang^{17,18}, Meng Wang^{17,18}, Qiuhong Wang⁷, Shaobo Wang^{2,21}, Siguang Wang¹⁹, Wei Wang^{5,4}, Xiuli Wang¹³, Xu Wang², Zhou Wang^{2,3,1}, Yuehuan Wei⁵, Mengmeng Wu⁴, Weihao Wu², Yuan Wu², Mengjiao Xiao², Xiang Xiao⁴, Binbin Yan¹, Xiyu Yan²², Yong Yang², Chunxu Yu²⁰, Ying Yuan², Zhe Yuan⁷, Youhui Yun², Xinning Zeng², Minzhen Zhang², Peng Zhang¹², Shibo Zhang², Shu Zhang⁴, Tao Zhang^{2,3}, Wei Zhang¹, Yang Zhang^{17,18}, Yingxin Zhang^{17,18}, Yuanyuan Zhang¹, Li Zhao^{2,3}, Jifang Zhou¹², Ning Zhou^{2,3}, Xiaopeng Zhou⁸, Yong Zhou¹⁰, Yubo Zhou², and Zhizhen Zhou²

(PandaX Collaboration)

- ¹New Cornerstone Science Laboratory, Tsung-Dao Lee Institute, Shanghai Jiao Tong University, Shanghai, 200240, China
- ²School of Physics and Astronomy, Shanghai Jiao Tong University, Key Laboratory for Particle Astrophysics and Cosmology (MoE), , Shanghai Key Laboratory for Particle Physics and Cosmology, Shanghai 200240, China
- ³Shanghai Jiao Tong University Sichuan Research Institute, Chengdu 610213, China
- ⁴School of Physics, Sun Yat-Sen University, Guangzhou 510275, China
- ⁵Sino-French Institute of Nuclear Engineering and Technology, Sun Yat-Sen University, Zhuhai, 519082, China
- ⁶Department of Physics, Yantai University, Yantai 264005, China
- ⁷Key Laboratory of Nuclear Physics and Ion-beam Application (MOE), Institute of Modern Physics, Fudan University, Shanghai 200433, China
- ⁸School of Physics, Beihang University, Beijing 102206, China
- ⁹Peng Huanwu Collaborative Center for Research and Education, Beihang University, Beijing 100191, China
- ¹⁰Beijing Key Laboratory of Advanced Nuclear Materials and Physics, Beihang University, Beijing 102206, China
- ¹¹Southern Center for Nuclear-Science Theory (SCNT), Institute of Modern Physics, Chinese Academy of Sciences, Huizhou 516000, China
- ¹²Yalong River Hydropower Development Company, Ltd., 288 Shuanglin Road, Chengdu 610051, China
- ¹³School of Mechanical Engineering, Shanghai Jiao Tong University, Shanghai 200240, China
- ¹⁴Department of Physics, University of Maryland, College Park, Maryland 20742, USA
- ¹⁵State Key Laboratory of Particle Detection and Electronics, University of Science and Technology of China, Hefei 230026, China
- ¹⁶Department of Modern Physics, University of Science and Technology of China, Hefei 230026, China
- ¹⁷Research Center for Particle Science and Technology, Institute of Frontier and Interdisciplinary Science, , Shandong University, Qingdao 266237, Shandong, China
- ¹⁸Key Laboratory of Particle Physics and Particle Irradiation of Ministry of Education, Shandong

University, , Qingdao 266237, Shandong, China

¹⁹State Key Laboratory of Nuclear Physics and Technology, School of Physics, Peking University, Beijing 100871, China

²⁰School of Physics, Nankai University, Tianjin 300071, China

²¹SJTU Paris Elite Institute of Technology, Shanghai Jiao Tong University, Shanghai, 200240, China

²²School of Physics and Astronomy, Sun Yat-Sen University, Zhuhai, 519082, China

February 7, 2024

Abstract

We propose a major upgrade to the existing PandaX-4T experiment in the China Jinping Underground Laboratory. The new experiment, PandaX-xT, will be a multi-ten-tonne liquid xenon, ultra-low background, and general-purpose observatory. The full-scaled PandaX-xT contains a 43-tonne liquid xenon active target. Such an experiment will significantly advance our fundamental understanding of particle physics and astrophysics. The sensitivity of dark matter direct detection will be improved by nearly two orders of magnitude compared to the current best limits, approaching the so-called “neutrino floor” for a dark matter mass above $10 \text{ GeV}/c^2$, providing a decisive test to the Weakly Interacting Massive Particle paradigm. By searching for the neutrino less double beta decay of ^{136}Xe isotope in the detector, the effective Majorana neutrino mass can be measured to a $[10 - 41] \text{ meV}/c^2$ sensitivity, providing a key test to the Dirac/Majorana nature of neutrinos. Astrophysical neutrinos and other ultra-rare interactions can also be measured and searched for with an unprecedented background level, opening up new windows of discovery. Depending on the findings, PandaX-xT will seek the next stage upgrade utilizing isotopic separation on natural xenon.

1 Introduction

Dark matter (DM) and neutrinos are crucial matter ingredients in the Universe, both playing key roles in the evolution of the Universe and the formation of galactic structures. However, their fundamental properties remain unsettled. One of the leading candidates of DM is the so-called “Weakly Interacting Massive Particles” (WIMPs). They emerge naturally from various extensions of the Standard Model of particle physics, for example, Supersymmetry, and can reproduce the observed DM relic density without fine-tuning [1, 2]. In 1985, inspired by the experimental development in searching for coherent neutrino mag-nucleus scatterings, Goodman and Witten proposed to use similar detectors to search for rare collisions between DM particles and atomic nuclei [3]. This experimental approach, known as the DM direct detection, has been carried out around the globe for nearly forty years (see, for example, Refs. [4, 5, 6, 7, 8, 9] and references therein). In recent years, the dual-phase xenon time projection chamber (TPC) has emerged as a leading experimental technique and made very fast progress on the detection sensitivity to DM-nucleon interactions, covering a wide range of parameter space for a DM mass greater than $5 \text{ GeV}/c^2$. Three large experimental collaborations, PandaX [10], XENON [11], and LZ [12] have now all entered the multi-tonne-target stage. Yet, no clear DM signals have been observed. Ultimately, the sensitivity of DM direct detection will be limited by the neutrino background from the coherent scatterings of solar and atmospheric neutrinos with nuclei, known as the “neutrino floor” [13] or “neutrino fog” [14]. It is worth noting that once the neutrino floor is reached, the xenon detector is also a sensitive probe of neutrino interactions, which offers new physics opportunities on its own.

The neutrino can be either different from or the same as its own anti-particle, known as the Dirac or Majorana fermion, respectively [15]. The Majorana nature of the neutrino would offer a natural explanation for the smallness of the neutrino mass via the so-called Seesaw mechanism [16, 17, 18, 19, 20], and may also be connected to the matter-antimatter asymmetry in the Universe through Leptogenesis [21]. It has been long realized that if neutrinos are Majorana fermions, an ultra-rare nuclear decay known as the Neutrinoless Double Beta Decay (NLDBD) will happen [22]. NLDBD experiments can probe the effective Majorana neutrino mass ($m_{\beta\beta}$), a linear combination of three neutrino mass eigenvalues therefore dependent on the neutrino mass ordering (MO) [23]. Over the years, quite many NLDBD experiments have been carried out. The most recent ones search for NLDBD with the sensitivity of $m_{\beta\beta}$ at $\mathcal{O}(100) \text{ meV}$ [24, 25, 26, 27, 28, 29, 30]. KamLAND-Zen, which uses 800 kg of enriched ^{136}Xe , has recently produced the best upper limit on $m_{\beta\beta}$ of $[36 - 156] \text{ meV}/c^2$ [30]. Some future experiments, such

*spokesperson: jianglai.liu@sjtu.edu.cn

as nEXO (^{136}Xe) [31], KamLAND2-ZEN (^{136}Xe) [32], LEGEND (^{76}Ge) [33], CDEX-300 ν (^{76}Ge) [34], JUNO-DBD ($^{130}\text{Te}/^{136}\text{Xe}$) [35], CUPID (^{100}Mo) [36], are aiming at a sensitivity of 15 meV/ c^2 or better, to fully cover the parameter space corresponding to the so-called inverted neutrino MO.

The DM direct detection and NLDBD experiments both pursue extremely low background and share similar detection techniques. However, due to vastly different energy regions and signal characteristics, and that NLDBD experiments normally require enriched isotopes and emphasize the energy resolution in the MeV region, the two types of experiments are mostly developed in parallel. Recently, securing large amounts of enriched isotopes for NLDBD searches has become a major challenge. On the other hand, XENON and LZ have demonstrated to achieve a sub-percent energy resolution around 2.5 MeV, the Q -value of ^{136}Xe NLDBD. Consequently, the approach of using a large natural xenon detector (containing $\sim 8.9\%$ ^{136}Xe) to simultaneously pursue both avenues becomes increasingly attractive [37, 38, 39].

The China Jinping underground Laboratory (CJPL), located in Sichuan Province, China, with an overburden of 2,400 m, is currently the deepest underground laboratory in the world [40]. The extreme depth provides superb shielding to cosmic rays and related background, ideal for the experimental studies of DM and neutrinos. Two main experiments, the PandaX [41, 42] and CDEX [43, 44, 45], have been developing staged research programs on the DM and neutrinos at CJPL since 2009. The previous two generations of PandaX featuring a 120 kg (PandaX-I) and 580 kg (PandaX-II) liquid xenon (LXe) TPC, respectively, had produced competitive results in dark matter search [46, 47, 48], as well as in neutrino studies [49]. PandaX-4T, with a sensitive target of 4 tonnes of LXe, is under operation in the newly expanded CJPL-II [50]. With only the commissioning data, it produced leading constraints to DM-nucleon and DM-electron interactions [10, 51, 52, 53] and the electromagnetic properties of the DM [54, 55], and made a precise determination of the two-neutrino double beta decay (DBD) lifetime of ^{136}Xe [56] and the best lower limits on the lifetimes of DBD and NLDBD of ^{134}Xe [57]. As CJPL-II is being transformed into a general-purpose National Major Scientific Facility in China, we propose a next-generation experiment, PandaX-xT, with a multi-ten-tonne active target, strategically combining the DM and NLDBD efforts. When reaching its full scale, PandaX-xT is envisioned to contain 47 tonnes of natural xenon, of which 43 tonnes function as the active target. The main scientific objectives of PandaX-xT include, but are not limited to:

1. Searching for DM-nucleon interactions with a sensitivity to the neutrino floor, a decisive test on the WIMP DM paradigm;
2. A stringent test on the Majorana nature of neutrinos using the NLDBD of ^{136}Xe , covering most of the parameter space for inverted neutrino MO;
3. Detecting low-energy neutrinos from the Sun and other astrophysical origins, and searching for ultra-rare new physics signals in general.

In the rest of this paper, we shall discuss the conceptual design of PandaX-xT, the background projections in different energy regions, and its scientific potential.

2 Conceptual Design of PandaX-xT

The overall design of the PandaX-xT is shown in Fig. 1, reusing most of the existing lab infrastructure from PandaX-4T. The LXe detector is located in the center of an outer ultrapure water veto (OVETO). To achieve an extremely low background environment, the LXe cryostat in which the TPC is placed is made with a thin-walled (~ 3 mm) ultrapure copper inner vessel (IV), with a double-walled vacuum insulated low background titanium outer vessel (OV). In between the IV and OV, a low-temperature liquid scintillator (LS) volume is pressurized to balance the internal pressure of the IV, but also acts as an anti-coincidence detector to suppress the background (IVETO). The layout of the TPC, IVETO, and OV is shown in Fig. 2. To satisfy the needs of detecting DM, NLDBD, and astroparticle neutrinos, PandaX-xT is required to have an effective energy range between 100 eV and 10 MeV, an energy resolution of $\sigma/E < 1\%$ at 2.5 MeV, and a sub-cm vertex resolution. The major detector components of PandaX-xT and key design features will be discussed below.

The OVETO utilizes the passive water shielding in PandaX-4T, contained in a stainless steel tank with a total volume of 900 m³. The radioactivity from the experimental hall is shielded by the water to a negligible level. The radioactivity of the water is measured during the PandaX-4T operation to be ~ 10 $\mu\text{Bq/kg}$ for ^{238}U , ^{232}Th , ^{40}K and ^{222}Rn , leading also to a negligible background contribution. We plan to instrument the water shielding with two layers of 8-inch PMTs, separated by Tyvek paper as optical reflectors. The inner layer serves as a neutron veto with some gamma vetoing capability. The inner PMTs will be mounted on the surface of a cylinder surrounding and looking toward the liquid xenon detector, providing a photocathode coverage of $\sim 10\%$. The neutrons are tagged by the 2.2 MeV gamma rays from hydrogen captures, and the tagging efficiency is estimated by a Geant4 [58] simulation to be about 70% assuming a trigger threshold of 5 fired PMTs. At a later stage, we plan to blend $\sim 5\%$ LS in the water using water-based liquid scintillator technology [59], to increase the light yield and therefore

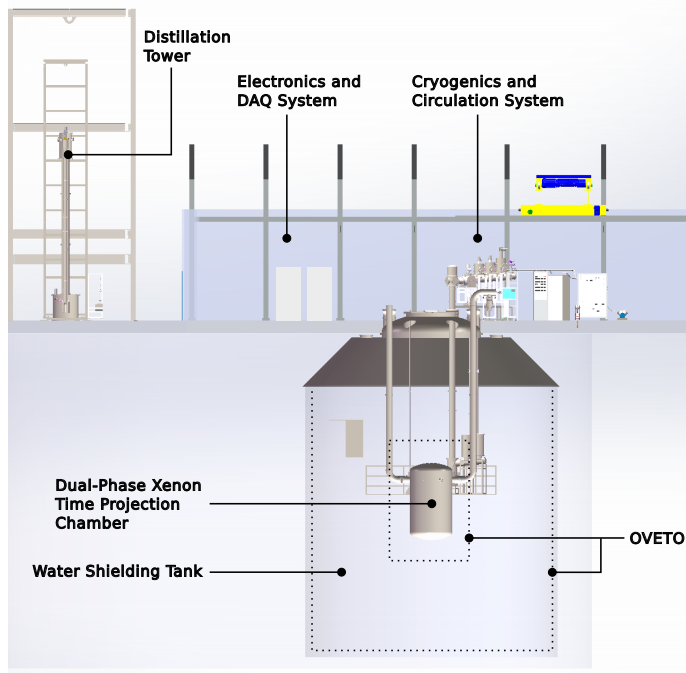


Figure 1: Schematics of the overall layout of PandaX-xT.

neutron tagging efficiency. The outer layer consists of PMTs mounted on the wall of the cylindrical water container in a sparser arrangement compared to the inner layer, providing a very high efficiency in vetoing cosmic rays and cosmic ray-induced hadronic showers. In addition, OVETO can help detect atmospheric neutrinos *in situ*. Such a measurement will reduce the systematic uncertainty of the “neutrino floor” prediction for dark matter mass larger than 10 GeV.

The IVETO is a layer of 0.5 m thick LS instrumented with plastic wavelength shifting (WLS) fibers coupled to an array of photosensors. The WLS fibers collect and shift the wavelength of the scintillation photons before sending them to the photosensors, a widely-used approach (see, e.g., Refs. [60, 61, 62, 63]). The neutron capture signals in LS or partial energy deposition from gamma rays from internal materials will be tagged to provide an effective veto for the otherwise candidate events happening in the TPC. The LS is cooled to the LXe temperature, pressure-balanced with the copper inner cryostat. Such a design was first used in EXO-200 [64], using cryogenic fluid outside the inner copper vessels, but without the veto function. The pressure balance allows a significant reduction in the thickness of the copper cryostat to minimize the radioactive background. At the LXe temperature, the LS stays as a thick translucent fluid, leading to a short scattering length thereby localized scintillation photons, which helps the photon collection by the WLS fibers and position reconstruction as demonstrated in the LiquidO project [65]. With a 200 keV threshold, the veto efficiency for low-energy neutron background events is estimated to be better than 90% via a simulation (Sec. 3).

The cryostat system holds the liquid xenon target and TPC at 178 K, with a maximum working pressure of 0.35 MPa, while preventing contamination by external radioactivity and electronegative impurity. To meet the low background requirements of the PandaX detector, as mentioned earlier the IV is made with a thin-walled oxygen-free copper container with a diameter of ~ 2.65 m and a total height of ~ 4 m containing the liquid xenon. The copper vessel thickness is kept thin to minimize its mass and radioactivity. The OV is a double-walled vacuum-insulated titanium vessel with an outer (inner) diameter of ~ 4 m (3.5 m) and an outer (inner) height of ~ 6 m (5 m). In between the IV and OV is a 0.5 m-thick LS IVETO region, with its pressure balanced with the liquid xenon, so the actual pressure is held by the OV. Special care has to be taken in the copper vessel design due to the non-uniform pressure caused by the LXe height, as well as in the control of pressure during the filling and emptying of the detector. The LXe TPC defines the active volume of the detector. Since the full-scale PandaX-xT will contain 43 tonnes of liquid xenon in the active volume, the TPC is ~ 2.6 m in diameter and ~ 3 m in height, confined by large and photon-transparent electrodes (the cathode, gate, and anode) made with wire grids or meshes. Dual-phase xenon TPC technology will be employed as the baseline technology, in which the ionization signal is converted into proportional scintillation in the gaseous xenon between the gate and anode. Alternative options, for example, with proportional scintillation produced in liquid xenon [66, 67, 68] will also be explored. Since xenon procurement will likely take some time, the volume of the TPC needs to be easily upgraded based on the amount of xenon in possession. An acrylic barrel will be used as the major structural holder of the TPC. There is a very good assurance on the low radioactivity since the acrylic panels used in JUNO have achieved a part-per-trillion (ppt) level of radio-impurity in mass production [69, 70]. The inner surface of

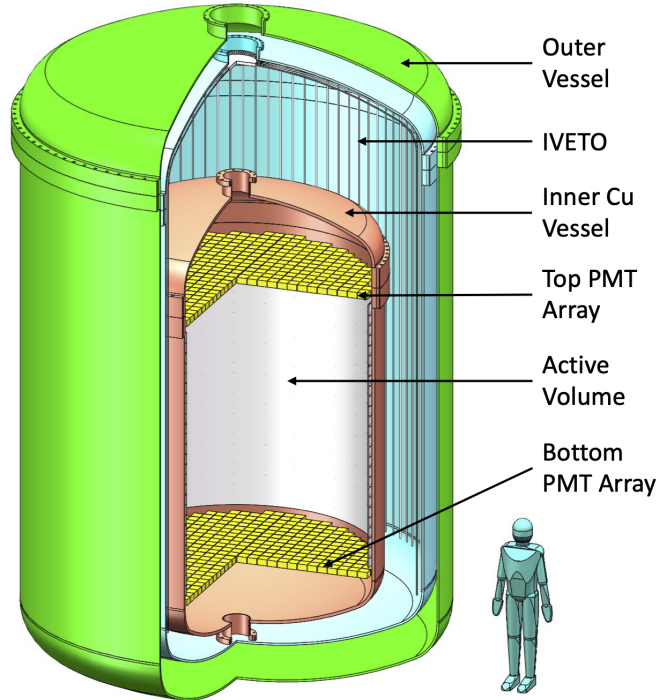


Figure 2: Schematic drawing of the conceptual design of the PandaX-xT cryostat and TPC.

the acrylic will be covered by a cylindrical sleeve of Polytetrafluoroethylene (PTFE) reflector to enhance the photon collection efficiency. The field-shaping circuitry will be implemented on a cylindrical flexible printed circuit board sandwiched between the PTFE sleeve and acrylic barrel. The top and bottom of the TPC will be enclosed by two acrylic plates which support the photosensor arrays. Such a design is sufficiently robust and straightforward to be fabricated. Assuming that the photosensor arrays are constructed into the final form, the acrylic barrel structure will be the only component that gets swapped for each upgrade. The basic TPC performance parameters are: 1) a photon detection efficiency of $>10\%$, 2) a drift field of >100 V/cm to allow for a 99.7% rejection of electron-recoil (ER) events, while maintaining a 50% efficiency on the DM-nuclear recoil (NR) events. These specifications have been mostly achieved in PandaX-II and PandaX-4T [47, 10].

The photosensor arrays collect the 178 nm photons produced in the liquid and gaseous xenon, providing energy measurement as well as locations and sequences of energy depositions. The photosensitive area of PandaX-xT will exceed 10 m². In the past, significant saturation effects were observed in the Hamamatsu R11410 3-inch photomultiplier tubes (PMTs) in the MeV regime [71, 56, 72], limiting the energy linearity and resolution, and impairing the ability to reconstruct scattering positions in the LXe TPCs. Compared to R11410, Silicon Photomultipliers (SiPMs) have much better granularity and energy linearity, but unfortunately with much higher dark count rates under the LXe temperature (best-reported value >0.1 Hz/mm² [73], at least one order of magnitude higher than that of R11410). The implementation of SiPM electronics would also be challenging due to the large number of channels. Therefore, a new type of high granularity photosensors with a pixel size of $\sim 2.5 \times 2.5$ cm² (Hamamatsu R12699) are being considered as the primary option for PandaX-xT. In total, we expect a total of ~ 8000 independent channels if both top and bottom arrays are instrumented with R12699. Their fast (\sim ns) timing (vs. ~ 3.5 ns for R11410) may also facilitate the separation of ER and NR events via pulse shape discrimination.

The readout electronics and data acquisition system digitizes the waveforms from photosensors and saves them on disk for future processing. They must support different data-taking rates in physics runs (~ 10 Hz) and calibration runs (>100 Hz). The readout system of PandaX-xT becomes much more challenging due to the large number of channels compared to PandaX-4T. The baseline solution involves using 500 MS/s 14-bit customized digitizers [74] which allows both single-channel-over-threshold readout or a firmware-based global readout trigger. Despite the maturity of the technology, it still needs to address the radioactivity and outgassing of thousands of mini-coaxial cables and the development of high-density low-temperature feedthroughs. As an alternative solution, cold electronics are under consideration for PandaX-xT. The system would be positioned near the photosensors inside the inner cryostat, digitize electrical signals and subsequently convert the data into optical signals using low-power transceivers. The system should feature high-speed sampling (> 100 MS/s) and low-power consumption (<100 mW/channel). Additionally, the front-end electronics should function fully at 178 K temperature and exhibit low radioactivity. The increasing sampling rate and expanding number of readout channels

present significant challenges in data processing and storage. During the standard background data taking, assuming the sampling rate of 500 MS/s, it is estimated that over 5 TB of raw data will be generated per day. An upgrade of the data reduction strategy developed for PandaX-4T has the potential to effectively address these challenges [75].

The LXe handling system for the filling, recovery, and storage of xenon, dubbed First-X, allows xenon transfer in and out of the PandaX-xT detector entirely under the liquid form [76]. This is imperative since the traditional filling and recuperation process with gaseous xenon becomes too time-consuming. The First-X system consists of multiple storage tanks, two cryogenic pumps, and the liquid nitrogen (LN2) and gas nitrogen (GN2) storage modules. Each storage tank is designed to store over 6 tonnes of xenon with an inner volume of 6.3 m³ and a design pressure of 7.1 MPa, satisfying the needs for long-term xenon storage in liquid phase (178 K, 0.2 MPa) or gaseous phase (300 K, 7.0 MPa). The storage tank's pressure can be rapidly regulated by three heat exchangers including two independent LN2-based cooling modules and one GN2-based heater. The cryogenic pump is a centrifugal pump with a magnetic drive that isolates the pump and LXe to avoid radioactivity contamination from the electric motor. The First-X system with six storage tanks has been constructed. The LXe filling/recovery mass flow rate has been demonstrated to reach 2.1 tonnes/hour.

The cryogenics and recirculation system provides cooling power for the LXe, while removing electronegative impurities with an active circulation loop and a purifier. The concept design is based on the successful operation of the cooling buses used in previous generations of PandaX [77, 78]. A preliminary estimate of the total heat load on the cryogenic system for PandaX-xT is about 1300 W at 178 K. Therefore a 1500 W cooling power is needed to achieve accurate control of the saturated vapor pressure of liquid xenon. A customized cooling tower with at least two GM Cryocoolers (Cryomech AL600) will be used to maintain the low-temperature operations at 178 K. Alternative means of cooling such as liquid nitrogen [79] will be incorporated via parallel cooling heads and loops. In addition, to achieve a long electron lifetime in the drifting field (>2 ms, corresponding to an electronegative impurity level of 10⁻¹⁰ mol/mol), a sufficiently fast recirculation speed is needed on both the liquid and gaseous xenon. The traditional gas recirculation with hot purifiers (~100 standard liters per minute, or slpm) and heat exchangers can be used with a customized magnetically-coupled piston gas pump. Moreover, since O₂ is usually the dominant contributor to the attenuation of ionized electrons in liquid xenon, the liquid xenon recirculation (~2 lpm) with a cryogenic pump and O₂ sorbent will be used in parallel. This approach has been demonstrated to work very effectively in XENONnT [80]. Special measures of radon control will be taken to avoid introducing radon into the TPC through the recirculation loops.

The distillation system removes the radioactive impurities such as ⁸⁵Kr, ²²²Rn and tritium from the xenon. Krypton and radon are noble gas impurities originating either from external leaks or internal emanations, which cannot be removed by commercial purifiers. Tritium background was introduced in PandaX-II and PandaX-4T through tritiated-methane calibration injection, and the removal efficiency from the commercial purifier also appeared insufficient for a tritium level below 10⁻²⁴ mol/mol [49, 10]. Cryogenic distillation is an effective technique to achieve ultra-pure xenon with a large flow rate based on the different boiling points of Xe, Kr, Rn, and tritiated methane (165 K, 120 K, 211 K and 111.5 K at atmosphere pressure, respectively), as demonstrated in earlier generations of PandaX [81, 82]. The requirements from PandaX-xT are more stringent (see Sec. 3), with levels of ⁸⁵Kr, ²²²Rn and tritium better than 2 nBq/kg, 0.5 μBq/kg, and 0.01 nBq/kg, respectively. A new krypton-removal tower and radon-removal tower are under construction. According to the design, the krypton content in xenon could be reduced to 1×10⁻¹⁴ mol/mol (2 nBq/kg) at the flow rate of 30 kg/h with 99 % xenon collection efficiency. The krypton tower is expected to remove tritium in the xenon to a completely negligible level. For the radon tower, with a 5 lpm liquid xenon flow rate (860 kg/h), the radon reduction could reach a factor of 10, which would be satisfactory assuming the best radon level in PandaX-4T (5 μBq/kg). These, together with other means of strict radioactivity control, are expected to lower the internal radioactive gas content to the desired values.

3 Background Estimation

The background level is the major driver of the scientific potential of PandaX-xT. For a multi-tonne LXe detector, there are three major classes of background, 1) background arising from detector materials, 2) internal background from ⁸⁵Kr, ²²²Rn, and tritium, and 3) physical background such as DBD events from ¹³⁶Xe and neutrino scattering events. The first component exhibits strong position dependence at the outskirts of the detector, so a proper fiducial volume selection can significantly reduce its contribution. The latter two components are uniformly distributed inside the detector. In this study, we assume that the background from the detector materials is primarily due to photosensor arrays and the copper vessel. The radioactivity levels are taken to be 0.02, 0.01 and 1.5 mBq/cm² for photosensors for ²³⁸U, ²³²Th, and ⁴⁰K, respectively, based on prototype sample measurements, and 5 ppt of ²³⁸U, ²³²Th, and ⁴⁰K for the copper vessel (achieved in Majorana Demonstrator, EXO-200, and SuperCDMS

experiments [83, 84, 85]). For the internal background in LXe, we assume a level of 2 nBq/kg and 0.5 μ Bq/kg for ^{85}Kr and ^{222}Rn , respectively. For the physical background, the rates and energy spectra are taken from Ref. [13], except those for the double electron-capture of ^{124}Xe , which are taken from the recent measurement from XENONnT [86]. The cosmogenically produced ^{137}Xe is assumed to be two orders less in comparison to that estimated in DARWIN [87], scaled using the total muon rate ratio between the CJPL and LNGS [88].

A customized Geant4 simulation, BambooMC [89], is used to estimate the background in PandaX-xT using a simplified geometry in Fig. 2. The approach is very similar to that for Pandax-4T [42, 90]. The intrinsic decay class in Geant4 is used to simulate radioactive decay chains, with all energy depositions inside the detector and veto detectors recorded, allowing a straightforward evaluation of the ER background. The neutron production arising from material radioactivities is simulated using a neutron generator improved from the traditional SOURCES-4A [91], which utilizes an updated nuclear cascade model and fission model implemented in Geant4 to properly take into account correlated emissions of neutron and gamma ray(s) as well as multiple neutrons [92, 89].

Four sets of cuts are developed in simulation to select candidates, namely the single-scatter cut, veto cuts, energy region of interest (ROI) cuts, and fiducial volume (FV) cuts:

1. Single-scatter cut rejects events with multiple energy depositions in the detector simulation.
2. Veto cuts remove events with energy deposition greater than 200 keV in the IVETO region. While the OVETO will operate at the same time providing additional veto efficiency, we omit its contribution in this study for conservativeness.
3. ROI cuts are defined for three main physics regions. The DM ROI, [1, 10] keV_{ee}, includes both low energy ER and NR background (neutron and neutrino-nuclear coherent scattering) events. The solar neutrino ROI, [10, 150] keV_{ee}, refers to the primary energy region for elastic-electron scattering signals from solar pp neutrinos. The NLDBD ROI, [2433, 2483] keV_{ee}, covers a 50-keV window around the Q -value of ^{136}Xe NLDBD (2458 keV). To implement a simplified energy response model, the ER energy deposition is smeared with a resolution function σ/E of $30\%/\sqrt{E/\text{keV}} + 0.4\%$. The NR energy is converted into an equivalent ER energy using the Lindhard formula [93] but without the smearing.
4. FV cuts are optimized with a simple “cut-and-count” figure-of-merit $\frac{\epsilon M \times T}{\sqrt{B}}$ in which ϵ is the signal efficiency, M is the fiducial mass, T is the data taking time, and B is the corresponding number of background events. For the DM ROI, since the signal is the DM-nucleus NR scattering, we assume an ER background rejection power of 99.7% and an NR acceptance of 50% with the standard ionization-to-scintillation ratio cut in LXe DM experiments. There is only ER background in the solar neutrino and NLDBD ROIs. The resulting optimized cylindrical FV for the DM and solar neutrino region is 34.2 tonne (190 mm to the top, 170 mm to the bottom, and 102 mm to the side of the TPC) and NLDBD is 8.4 tonne (780 mm to the top, 816 mm to the bottom, and 484 mm to the side of the TPC) of natural xenon.

After these cuts, background energy spectra below 150 keV (the DM and solar neutrino-electron scattering regions) and the high energy NLDBD region are shown in Figs. 3 and 4. Corresponding background events in the DM, solar neutrino, and NLDBD energy regions are summarized in Tables 1, 2, and 3. Note that the background rate in the NLDBD ROI is highly sensitive to the background assumption, so the results of a “baseline” and “ideal” assumption are given. Under the “baseline” assumption, the dominating background arises from the ^{214}Bi β -decay, the daughters of the internal ^{222}Rn daughter. Although ^{214}Bi can be very efficiently tagged and vetoed via the delayed coincidence of ^{214}Bi – ^{214}Po decay, we assume a 0.1% residual untagged ^{214}Bi nevertheless. Under the “ideal” assumption, we assume that the material background is reduced by 5 times from the “baseline” and the background from ^{222}Rn is negligible.

Table 1: Expected background for the DM search region between 1 to 10 keV_{ee}. The FV mass is 34.2 tonnes.

	ER (1/tonne/year)	NR (1/tonne/year)
Photosensors	8.4	0.0004
Copper vessel	0.1	0.0001
^{85}Kr	1.2	-
^{222}Rn	28.2	-
^{136}Xe	9.6	-
Solar ν	27.5	-
Atmospheric ν	0.0	0.02
Diffusive supernova ν	0.0	0.002
Total	75.0	0.02

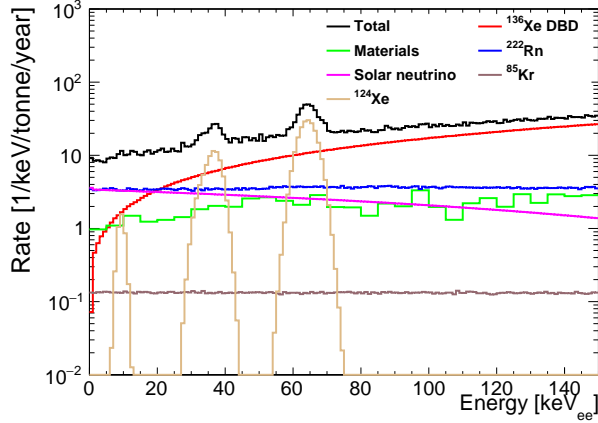


Figure 3: The energy spectra of individual background components between 1 and 150 keV (DM and solar neutrino regions) with veto applied.

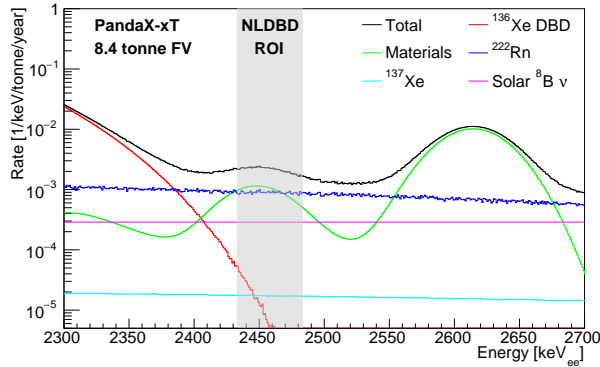


Figure 4: The energy spectra of individual background components in the MeV region under the “baseline” background assumption. See text for details.

4 Physics potential

Being a unique deep underground and ultralow background liquid xenon observatory, the physics potential of PandaX-xT is very rich. Instead of presenting an exhaustive list of physics, we benchmark the capability of PandaX-xT in the WIMP search, NLDBD, and solar neutrino detection, covering an effective energy range from keV to MeV. Within these energy windows, the sensitivity of alternative signals with a single-scattering nature can be estimated based on the background rate presented in the previous section. The sensitivities to more exotic signals, for example, with multiple energy depositions via nuclear or atomic excitations or with time correlations, have to be studied case by case and are beyond the scope of this paper.

For the WIMP search in the DM ROI, the background level is 75 events/tonne/year for electron recoil (ER) and 0.02 events/tonne/year for nuclear recoil (NR), respectively (Table 1). With the simple “cut-and-count” assumptions of an ER background rejection power of 99.7% and an NR acceptance of 50%, the ER and NR backgrounds in the ROI are 0.23 events/tonne/year and 0.01 events/tonne/year, respectively. With the standard DM halo and nuclear form factors parameters, and the spin-independent or spin-dependent isospin-conserving DM-nucleon interaction [94], and with a projected exposure of 200 tonne-year, the sensitivities are summarized in Fig. 5. Note that the PandaX-xT sensitivity reached a few times 10^{-49} cm² for spin-independent interactions at a DM mass of 40 GeV/ c^2 . The sensitivity is expected to improve with a likelihood approach with the full distributions of the signal and background incorporated. Nevertheless, the limit covers most of the allowed parameter space from the constrained minimal Supersymmetry models [95]. Also overlaid is the neutrino-background-only sensitivity “floor” with three neutrino-nucleus coherent scattering events from Ref. [13]. The sensitivities to the spin-dependent interactions with the proton and neutron are also given in the figure.

For NLDBD, at the Q -value of ^{136}Xe NLDBD (2458 keV), and with an energy resolution σ/E of better than 1%, the level of the background for the 8.4-tonne fiducial volume is 2.1×10^{-3} count/keV/tonne/year

Table 2: Expected background for the solar neutrino-electron elastic scattering region between 10 to 150 keV for the 34.2-tonne FV.

	ER (1/tonne/year)
Photosensors	270
Copper vessel	21
^{85}Kr	19
^{222}Rn	439
^{136}Xe	1927
^{124}Xe	276
Solar ν	343
Total	3295

Table 3: Expected background under the baseline and ideal scenarios for the NLDBD energy range between 2433 and 2483 keV for the 8.4-tonne FV. See text for details.

	Baseline (1/tonne/year)	Ideal (1/tonne/year)
Photosensors	1.4×10^{-2}	2.8×10^{-3}
Copper vessel	3.2×10^{-2}	6.3×10^{-3}
^{222}Rn	4.5×10^{-2}	-
^{136}Xe DBD	5.2×10^{-4}	5.2×10^{-4}
^{137}Xe	8.7×10^{-4}	8.7×10^{-4}
Solar ^8B ν	1.4×10^{-2}	1.4×10^{-2}
Total	1.1×10^{-1}	2.4×10^{-2}

within a 50 keV energy window (Table 3). The sensitivity to the NLDBD half-life can be expressed as

$$T_{1/2}^{\text{NLDBD}} = \frac{\ln 2 \times \epsilon \times f_{\text{ROI}} \times (\# \text{ of } ^{136}\text{Xe} \text{ atoms}) \times T}{1.64\sqrt{B}}, \quad (1)$$

in which $f_{\text{ROI}} \sim 0.7$ is the fraction of events enclosed in the NLDBD ROI, ϵ is the signal selection efficiency which is assumed to be nearly 100%, B is the number of background events (Table 3), and $T = 10$ -year. This leads to a half-life sensitivity of 3.3×10^{27} and 6.9×10^{27} years for the baseline and ideal background assumptions, respectively. The baseline result corresponds to an upper limit of the effective Majorana mass between $[10 - 41]$ meV/ c^2 on $m_{\beta\beta}$, in which the spread is due to the uncertainty in the nuclear matrix elements [102]. The sensitivity can mostly cover the allowed space for inverted neutrino MO, assuming that NLDBD is mediated by light Majorana neutrinos, as illustrated in Fig. 6.

For the solar neutrinos, we benchmark our sensitivity to the solar ^8B neutrino fluxes via coherent elastic neutrino-nucleus scattering (CE ν NS), and the pp neutrino flux via neutrino-electron elastic scattering. With 200 tonne-year exposure, the number of detected ^8B neutrino CE ν NS events is approximately 710, conservatively estimated based on the PandaX-4T efficiency curve in a specialized low energy analysis in Ref. [96]. With an additional assumption of an equal number of accidental background events, PandaX-xT is capable of making a better-than 10% precision measurement on the ^8B neutrino fluxes (Fig. 7). We expect the efficiency and accidental background to be further improved along the way. For the pp neutrinos, assuming a 2% systematic uncertainty for material, krypton and radon background, the pp flux can be determined to $(6.0 \pm 0.2) \times 10^{10}$ cm $^{-2}$ s $^{-1}$ using ER spectra fitting, better than the current best measurement from Borexino [103].

Note that the neutrino scattering rate in Tables 1 and 2 has assumed standard electroweak interaction only. If there is an enhanced neutrino magnetic moment μ_ν due to the Majorana nature or exotic new physics beyond the SM, the elastic scattering cross section will be modified by a term [13]

$$\left(\frac{d\sigma}{dT}\right)_{\mu_\nu} = \frac{\pi\alpha_{\text{EM}}^2\mu_\nu^2}{m_e^2} \left[\frac{1 - T/E_\nu}{T} \right], \quad (2)$$

in which $\alpha_{\text{EM}} = 1/137$, m_e is the mass of the electron, and E_ν and T are the kinetic energy of the neutrino and recoiling electron, respectively. Therefore, the low energy pp neutrino measurement can be in turn used to search for μ_ν . With 200 tonne-year exposure and our background presented, we expect to achieve an unprecedented sensitivity of $1.2 \times 10^{-12} \mu_B$ to μ_ν (Fig. 8), where μ_B is the Bohr magneton.

5 Discussions and Conclusions

Besides the standard methods of background rejections through data selection cuts, new methods are also being pursued by the PandaX collaboration. We plan to make use of different scintillation timing

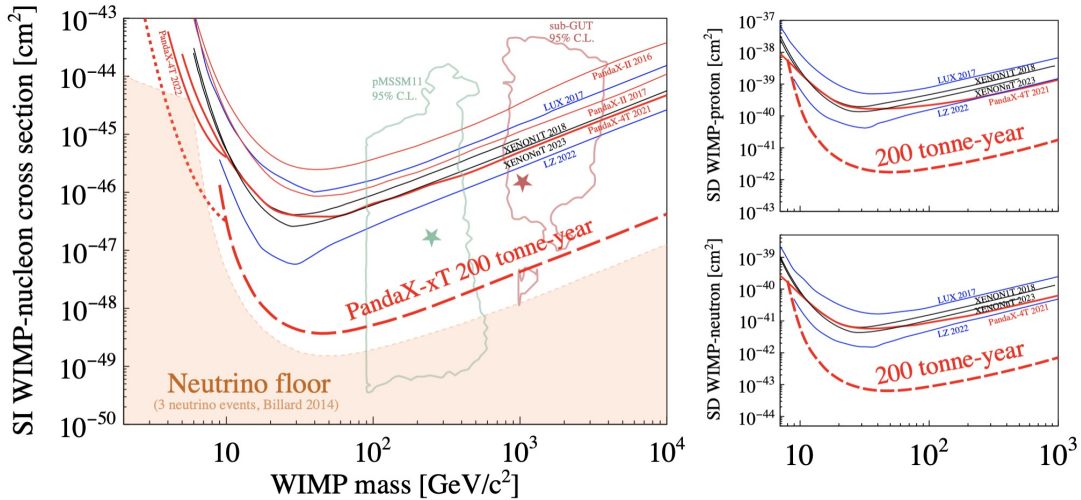


Figure 5: Projected sensitivities (red dashed curve) of PandaX-xT to spin-independent, and spin-dependent WIMP-neutron/-proton interactions estimated with a cut-and-count method, assuming the background level from Table 1, a 99.7% ER rejection power and a 50% NR acceptance, and an exposure of 200 tonne-year. Our benchmark energy range from 1 to 10 keV_{ee} has limited our sensitivity to DM masses less than 10 GeV/ c^2 . The sensitivity curve for low-mass DM below 10 GeV/ c^2 (dotted line in the left graph) is estimated based on the PandaX-4T efficiency curve in a specialized low energy analysis in Ref. [96], and a 1:1 ratio of ^8B neutrino induced CE ν NS and accidental coincidence background. The “neutrino floor” (3 events) and 95% C.L. contour of allowed parameter space in Supersymmetry models are taken from Refs. [13] and [97], respectively. Past experimental constraints [10, 48, 47, 98, 99, 51, 100, 101, 11, 12] are also overlaid.

profiles due to different fractions of 3 ns/20 ns decay components between the ER and NR to gain extra background rejection power in keV energy region [111]. In the spatial dimension, we plan to reconstruct individual scattering vertices to a sub-centimeter resolution, and even identify track features in β s, to reduce the background in the MeV energy region. Taking further advantage of the photosensors with \sim ns timing response, we plan to investigate the detection of Cherenkov photons using both temporal and spatial information, a new method for background discrimination in the MeV region [112].

CJPL is being transformed into a mature national facility [50], and most of the infrastructure from PandaX-4T will be inherited. These will ease the deployment of PandaX-xT. The CJPL site provides additional key advantages to PandaX-xT. The large overburden gives a much lower cosmogenic background, in particular ^{137}Xe . The low latitude (28°N) of CJPL, thereby higher field strength parallel to the earth’s surface, suppresses low energy cosmic rays entering the atmosphere. This leads to a more than two times lower atmospheric neutrino background, the “ultimate” background for DM direct detection in the high mass region (>10 GeV/ c^2), than those of high-latitude underground laboratories (LNGS, SURF, and SNOLAB) [113, 114]. Note that the prediction of the atmospheric neutrino flux and spectrum has rather large uncertainty. The PandaX-xT OVETO, with a volume of 900 m³, enables an measurement of atmospheric neutrino flux at CJPL.

PandaX-xT is envisioned to be carried out in multiple phases. In the first phase, natural xenon will be used as the detection target. We will gradually upgrade the detector based on the xenon in possession, reach a total target mass of 43 tonnes and operate for more than 10 years. In the next phase, we envision that isotopic separation technology will be used to produce xenon with artificially modified isotopic abundance (AMIA), either via a split of odd and even nuclei [115], or further enrichment of ^{136}Xe . Two functionally identical detectors can be filled with different AMIA xenon, and the sensitivity to spin-dependent properties of DM-nucleon interactions and NLDBD could be greatly improved by the “dual-detector mode”. It also provides a powerful way to probe parameter spaces below the neutrino floor, since the neutrino-nucleus coherent scattering is mostly spin-independent.

To summarize, we have demonstrated that the proposed PandaX-xT detector, with a 43 tonne active xenon target, will be a cutting-edge and multi-purpose observatory covering a wide range of physics topics in particle physics and astrophysics. With an exposure of 200 tonne-year, it allows a most sensitive search for DM-nucleon interactions to the neutrino floor [13, 14], a decisive test on the WIMP DM. The same detector, operated for 10 years, will provide stringent tests on the Majorana nature of neutrinos using the NLDBD of ^{136}Xe , effectively covering most of the parameter space for inverted neutrino MO. With its uniqueness in detecting low energy recoils, PandaX-xT will also allow precise detection of solar ^8B and pp neutrinos, as well as other neutrinos with astrophysical origins. These neutrinos can be used to broadly search for new physics, as well as in the context of multi-messenger astronomy.

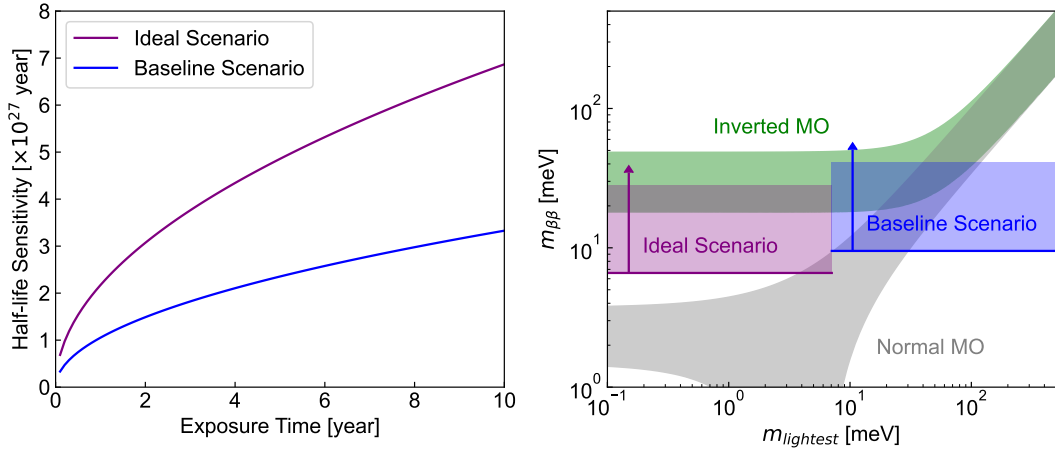


Figure 6: (Left) Projected 90% C.L. sensitivity to NLDBD half-life as a function of exposure time for the baseline and ideal scenarios. Inputs used in the calculation are in Table 3 and discussed in the text. (Right) Effective Majorana mass ($m_{\beta\beta}$) sensitivity with 10 year of exposure with respect to the phase space of the inverted and normal MO of neutrinos. The sensitivity bands of the two scenarios are due to the spread of commonly-used nuclear matrix elements. The two sensitivity bands are staggered intentionally for better visibility.

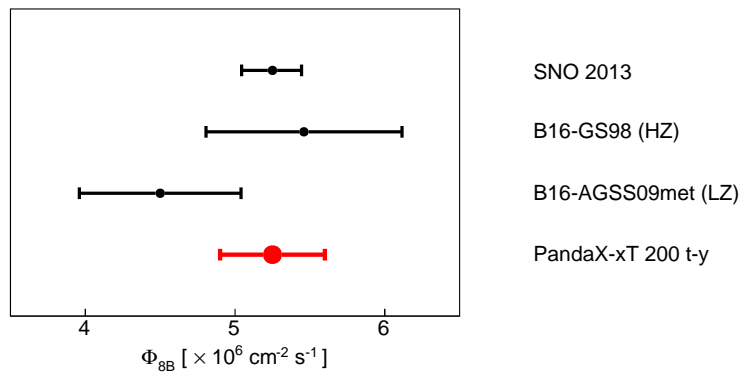


Figure 7: Projected sensitivity of PandaX-xT to solar ^8B neutrino flux assuming the same mean value as SNO [104], compared with theoretical models [105].

6 Acknowledgement

This project is supported in part by the Office of Science and Technology, Shanghai Municipal Government (grant Nos. 23JC1410200 and 22JCJC1410200), the Ministry of Science and Technology of China (grant No. 2023YFA1606200), and the National Science Foundation of China (grant Nos. 1209060, 12005131, 11905128, 11925502, 12222505, 12175139). We thank support from Double First Class Plan of the Shanghai Jiao Tong University, and the Tsung-Dao Lee Institute Experimental Platform Development Fund. We also thank the sponsorship from the Hongwen Foundation in Hong Kong, Tencent and New Cornerstone Science Foundation in China, and Yangyang Development Fund. Finally, we thank the CJPL administration and the Yalong River Hydropower Development Company Ltd. for indispensable logistical support and other help.

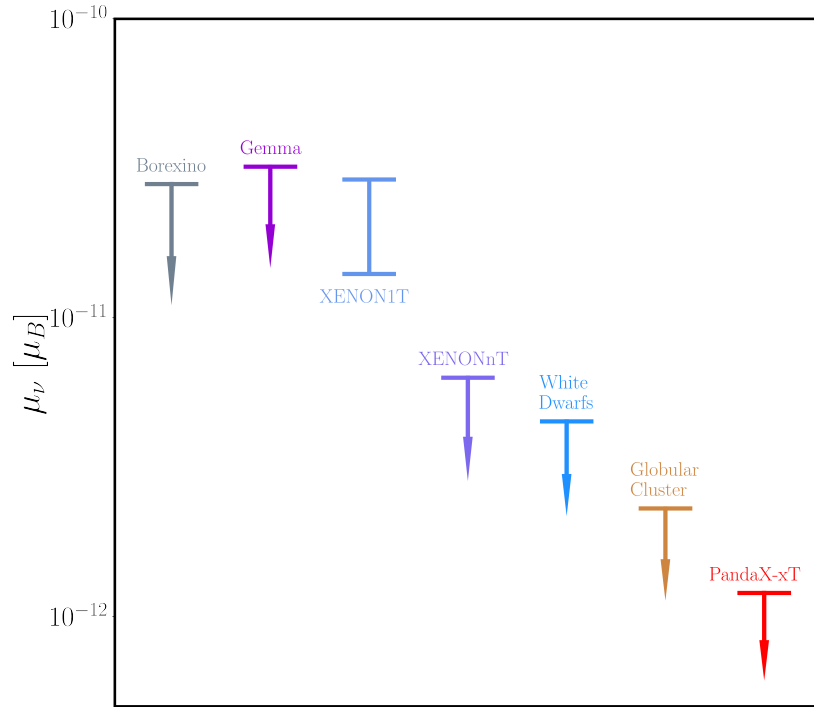


Figure 8: The sensitivity on the neutrino magnetic moment (90% C.L.) of PandaX-xT with 200 tonne-year exposure (red), together with constraints from current leading experiments [106, 80, 107] and astrophysical observations [108, 109], as well as a potential positive interpretation from Ref. [110]).

References

- [1] G. Bertone, D. Hooper, J. Silk, Particle dark matter: Evidence, candidates and constraints, *Phys. Rept.* 405 (2005) 279–390. [arXiv:hep-ph/0404175](#), [doi:10.1016/j.physrep.2004.08.031](#).
- [2] G. Jungman, M. Kamionkowski, K. Griest, Supersymmetric dark matter, *Phys. Rept.* 267 (1996) 195–373. [arXiv:hep-ph/9506380](#), [doi:10.1016/0370-1573\(95\)00058-5](#).
- [3] M. W. Goodman, E. Witten, Detectability of Certain Dark Matter Candidates, *Phys. Rev. D* 31 (1985) 3059. [doi:10.1103/PhysRevD.31.3059](#).
- [4] R. J. Gaitskell, Direct detection of dark matter, *Ann. Rev. Nucl. Part. Sci.* 54 (2004) 315–359. [doi:10.1146/annurev.nucl.54.070103.181244](#).
- [5] T. Marrodán Undagoitia, L. Rauch, Dark matter direct-detection experiments, *J. Phys. G* 43 (1) (2016) 013001. [arXiv:1509.08767](#), [doi:10.1088/0954-3889/43/1/013001](#).
- [6] J. Liu, X. Chen, X. Ji, Current status of direct dark matter detection experiments, *Nature Phys.* 13 (3) (2017) 212–216. [arXiv:1709.00688](#), [doi:10.1038/nphys4039](#).
- [7] M. Schumann, Direct Detection of WIMP Dark Matter: Concepts and Status, *J. Phys. G* 46 (10) (2019) 103003. [arXiv:1903.03026](#), [doi:10.1088/1361-6471/ab2ea5](#).
- [8] J. Billard, et al., Direct detection of dark matter—APPEC committee report, *Rept. Prog. Phys.* 85 (5) (2022) 056201. [arXiv:2104.07634](#), [doi:10.1088/1361-6633/ac5754](#).
- [9] P. Cushman, et al., Working Group Report: WIMP Dark Matter Direct Detection, in: *Snowmass 2013: Snowmass on the Mississippi*, 2013. [arXiv:1310.8327](#).
- [10] Y. Meng, et al., Dark Matter Search Results from the PandaX-4T Commissioning Run, *Phys. Rev. Lett.* 127 (26) (2021) 261802. [arXiv:2107.13438](#), [doi:10.1103/PhysRevLett.127.261802](#).
- [11] E. Aprile, et al., First Dark Matter Search with Nuclear Recoils from the XENONnT Experiment, *Phys. Rev. Lett.* 131 (4) (2023) 041003. [arXiv:2303.14729](#), [doi:10.1103/PhysRevLett.131.041003](#).
- [12] J. Aalbers, et al., First Dark Matter Search Results from the LUX-ZEPLIN (LZ) Experiment, *Phys. Rev. Lett.* 131 (4) (2023) 041002. [arXiv:2207.03764](#), [doi:10.1103/PhysRevLett.131.041002](#).
- [13] J. Billard, L. Strigari, E. Figueroa-Feliciano, Implication of neutrino backgrounds on the reach of next generation dark matter direct detection experiments, *Phys. Rev. D* 89 (2) (2014) 023524. [arXiv:1307.5458](#), [doi:10.1103/PhysRevD.89.023524](#).
- [14] C. A. J. O’Hare, New Definition of the Neutrino Floor for Direct Dark Matter Searches, *Phys. Rev. Lett.* 127 (25) (2021) 251802. [arXiv:2109.03116](#), [doi:10.1103/PhysRevLett.127.251802](#).

- [15] E. Majorana, Teoria simmetrica dell'elettrone e del positrone, *Nuovo Cim.* 14 (1937) 171–184. [doi:10.1007/BF02961314](https://doi.org/10.1007/BF02961314).
- [16] P. Minkowski, $\mu \rightarrow e\gamma$ at a Rate of One Out of 10^9 Muon Decays?, *Phys. Lett. B* 67 (1977) 421–428. [doi:10.1016/0370-2693\(77\)90435-X](https://doi.org/10.1016/0370-2693(77)90435-X).
- [17] T. Yanagida, Proc. workshop on unified theory and the baryon number in the universe, KEK Report No. 79-18 95.
- [18] M. Gell-Mann, P. Ramond, R. Slansky, Complex Spinors and Unified Theories, *Conf. Proc. C* 790927 (1979) 315–321. [arXiv:1306.4669](https://arxiv.org/abs/1306.4669).
- [19] S. L. Glashow, The Future of Elementary Particle Physics, *NATO Sci. Ser. B* 61 (1980) 687. [doi:10.1007/978-1-4684-7197-7_15](https://doi.org/10.1007/978-1-4684-7197-7_15).
- [20] R. N. Mohapatra, G. Senjanovic, Neutrino Mass and Spontaneous Parity Nonconservation, *Phys. Rev. Lett.* 44 (1980) 912. [doi:10.1103/PhysRevLett.44.912](https://doi.org/10.1103/PhysRevLett.44.912).
- [21] M. Fukugita, T. Yanagida, Baryogenesis Without Grand Unification, *Phys. Lett. B* 174 (1986) 45–47. [doi:10.1016/0370-2693\(86\)91126-3](https://doi.org/10.1016/0370-2693(86)91126-3).
- [22] W. H. Furry, On transition probabilities in double beta-disintegration, *Phys. Rev.* 56 (1939) 1184–1193. [doi:10.1103/PhysRev.56.1184](https://doi.org/10.1103/PhysRev.56.1184).
- [23] M. Agostini, G. Benato, J. A. Detwiler, J. Menéndez, F. Vissani, Toward the discovery of matter creation with neutrinoless $\beta\beta$ decay, *Rev. Mod. Phys.* 95 (2) (2023) 025002. [arXiv:2202.01787](https://arxiv.org/abs/2202.01787), [doi:10.1103/RevModPhys.95.025002](https://doi.org/10.1103/RevModPhys.95.025002).
- [24] M. Agostini, et al., Final Results of GERDA on the Search for Neutrinoless Double- β Decay, *Phys. Rev. Lett.* 125 (25) (2020) 252502. [arXiv:2009.06079](https://arxiv.org/abs/2009.06079), [doi:10.1103/PhysRevLett.125.252502](https://doi.org/10.1103/PhysRevLett.125.252502).
- [25] I. J. Arnquist, et al., Final Result of the Majorana Demonstrator’s Search for Neutrinoless Double- β Decay in Ge76, *Phys. Rev. Lett.* 130 (6) (2023) 062501. [arXiv:2207.07638](https://arxiv.org/abs/2207.07638), [doi:10.1103/PhysRevLett.130.062501](https://doi.org/10.1103/PhysRevLett.130.062501).
- [26] G. Anton, et al., Search for Neutrinoless Double- β Decay with the Complete EXO-200 Dataset, *Phys. Rev. Lett.* 123 (16) (2019) 161802. [arXiv:1906.02723](https://arxiv.org/abs/1906.02723), [doi:10.1103/PhysRevLett.123.161802](https://doi.org/10.1103/PhysRevLett.123.161802).
- [27] D. Q. Adams, et al., Search for Majorana neutrinos exploiting millikelvin cryogenics with CUORE, *Nature* 604 (7904) (2022) 53–58. [arXiv:2104.06906](https://arxiv.org/abs/2104.06906), [doi:10.1038/s41586-022-04497-4](https://doi.org/10.1038/s41586-022-04497-4).
- [28] V. Albanese, et al., The SNO+ experiment, *JINST* 16 (08) (2021) P08059. [arXiv:2104.11687](https://arxiv.org/abs/2104.11687), [doi:10.1088/1748-0221/16/08/P08059](https://doi.org/10.1088/1748-0221/16/08/P08059).
- [29] R. Arnold, et al., Results of the search for neutrinoless double- β decay in ^{100}Mo with the NEMO-3 experiment, *Phys. Rev. D* 92 (7) (2015) 072011. [arXiv:1506.05825](https://arxiv.org/abs/1506.05825), [doi:10.1103/PhysRevD.92.072011](https://doi.org/10.1103/PhysRevD.92.072011).
- [30] S. Abe, et al., Search for the Majorana Nature of Neutrinos in the Inverted Mass Ordering Region with KamLAND-Zen, *Phys. Rev. Lett.* 130 (5) (2023) 051801. [arXiv:2203.02139](https://arxiv.org/abs/2203.02139), [doi:10.1103/PhysRevLett.130.051801](https://doi.org/10.1103/PhysRevLett.130.051801).
- [31] G. Adhikari, et al., nEXO: neutrinoless double beta decay search beyond 10^{28} year half-life sensitivity, *J. Phys. G* 49 (1) (2022) 015104. [arXiv:2106.16243](https://arxiv.org/abs/2106.16243), [doi:10.1088/1361-6471/ac3631](https://doi.org/10.1088/1361-6471/ac3631).
- [32] R. Nakamura, H. Sambonsugi, K. Shiraiishi, Y. Wada, Research and development toward KamLAND2-Zen, *J. Phys. Conf. Ser.* 1468 (1) (2020) 012256. [doi:10.1088/1742-6596/1468/1/012256](https://doi.org/10.1088/1742-6596/1468/1/012256).
- [33] R. Brugnera, Neutrinoless double beta decay search with LEGEND, *PoS NOW2022* (2023) 075. [doi:10.22323/1.421.0075](https://doi.org/10.22323/1.421.0075).
- [34] H. Ma, W. Dai, L. Yang, CDEX-300 ν program for Ge-76 neutrinoless double beta decay search, *PoS TAUP2023* (2024) 200. [doi:10.22323/1.441.0200](https://doi.org/10.22323/1.441.0200).
- [35] J. Zhao, L.-J. Wen, Y.-F. Wang, J. Cao, Physics potential of searching for $0\nu\beta\beta$ decays in JUNO, *Chin. Phys. C* 41 (5) (2017) 053001. [arXiv:1610.07143](https://arxiv.org/abs/1610.07143), [doi:10.1088/1674-1137/41/5/053001](https://doi.org/10.1088/1674-1137/41/5/053001).
- [36] K. Alfonso, et al., CUPID: The Next-Generation Neutrinoless Double Beta Decay Experiment, *J. Low Temp. Phys.* 211 (5-6) (2023) 375–383. [doi:10.1007/s10909-022-02909-3](https://doi.org/10.1007/s10909-022-02909-3).
- [37] J. Aalbers, et al., A next-generation liquid xenon observatory for dark matter and neutrino physics, *J. Phys. G* 50 (1) (2023) 013001. [arXiv:2203.02309](https://arxiv.org/abs/2203.02309), [doi:10.1088/1361-6471/ac841a](https://doi.org/10.1088/1361-6471/ac841a).
- [38] J. Aalbers, et al., DARWIN: towards the ultimate dark matter detector, *JCAP* 11 (2016) 017. [arXiv:1606.07001](https://arxiv.org/abs/1606.07001), [doi:10.1088/1475-7516/2016/11/017](https://doi.org/10.1088/1475-7516/2016/11/017).
- [39] XLZD: Joining forces towards a next-generation Dark Matter experiment, <https://darwin.physik.uzh.ch/news.html>, <https://xlzd.org>.
URL <https://darwin.physik.uzh.ch/news.html>, <https://xlzd.org>

- [40] J.-P. Cheng, et al., The China Jinping Underground Laboratory and its Early Science, *Ann. Rev. Nucl. Part. Sci.* 67 (2017) 231–251. [arXiv:1801.00587](#), [doi:10.1146/annurev-nucl-102115-044842](#).
- [41] X. Cao, et al., PandaX: A Liquid Xenon Dark Matter Experiment at CJPL, *Sci. China Phys. Mech. Astron.* 57 (2014) 1476–1494. [arXiv:1405.2882](#), [doi:10.1007/s11433-014-5521-2](#).
- [42] H. Zhang, et al., Dark matter direct search sensitivity of the PandaX-4T experiment, *Sci. China Phys. Mech. Astron.* 62 (3) (2019) 31011. [arXiv:1806.02229](#), [doi:10.1007/s11433-018-9259-0](#).
- [43] K.-J. Kang, et al., Introduction to the CDEX experiment, *Front. Phys. (Beijing)* 8 (2013) 412–437. [arXiv:1303.0601](#), [doi:10.1007/s11467-013-0349-1](#).
- [44] Q. Yue, et al., Limits on light WIMPs from the CDEX-1 experiment with a p-type point-contact germanium detector at the China Jinping Underground Laboratory, *Phys. Rev. D* 90 (2014) 091701. [arXiv:1404.4946](#), [doi:10.1103/PhysRevD.90.091701](#).
- [45] H. Jiang, et al., Limits on Light Weakly Interacting Massive Particles from the First 102.8 kg × day Data of the CDEX-10 Experiment, *Phys. Rev. Lett.* 120 (24) (2018) 241301. [arXiv:1802.09016](#), [doi:10.1103/PhysRevLett.120.241301](#).
- [46] M. Xiao, et al., First dark matter search results from the PandaX-I experiment, *Sci. China Phys. Mech. Astron.* 57 (2014) 2024–2030. [arXiv:1408.5114](#), [doi:10.1007/s11433-014-5598-7](#).
- [47] A. Tan, et al., Dark Matter Results from First 98.7 Days of Data from the PandaX-II Experiment, *Phys. Rev. Lett.* 117 (12) (2016) 121303. [arXiv:1607.07400](#), [doi:10.1103/PhysRevLett.117.121303](#).
- [48] X. Cui, et al., Dark Matter Results From 54-Ton-Day Exposure of PandaX-II Experiment, *Phys. Rev. Lett.* 119 (18) (2017) 181302. [arXiv:1708.06917](#), [doi:10.1103/PhysRevLett.119.181302](#).
- [49] X. Zhou, et al., A Search for Solar Axions and Anomalous Neutrino Magnetic Moment with the Complete PandaX-II Data, *Chin. Phys. Lett.* 38 (1) (2021) 011301, [Erratum: *Chin. Phys. Lett.* 38, 109902 (2021)]. [arXiv:2008.06485](#), [doi:10.1088/0256-307X/38/10/109902](#).
- [50] J. Li, X. Ji, W. Haxton, J. S. Y. Wang, The second-phase development of the China JinPing underground Laboratory, *Phys. Procedia* 61 (2015) 576–585. [doi:10.1016/j.phpro.2014.12.055](#).
- [51] Z. Huang, et al., Constraints on the axial-vector and pseudo-scalar mediated WIMP-nucleus interactions from PandaX-4T experiment, *Phys. Lett. B* 834 (2022) 137487. [arXiv:2208.03626](#), [doi:10.1016/j.physletb.2022.137487](#).
- [52] S. Li, et al., Search for Light Dark Matter with Ionization Signals in the PandaX-4T Experiment, *Phys. Rev. Lett.* 130 (26) (2023) 261001. [arXiv:2212.10067](#), [doi:10.1103/PhysRevLett.130.261001](#).
- [53] D. Huang, et al., Search for Dark-Matter–Nucleon Interactions with a Dark Mediator in PandaX-4T, *Phys. Rev. Lett.* 131 (19) (2023) 191002. [arXiv:2308.01540](#), [doi:10.1103/PhysRevLett.131.191002](#).
- [54] X. Ning, et al., Limits on the luminance of dark matter from xenon recoil data, *Nature* 618 (7963) (2023) 47–50. [doi:10.1038/s41586-023-05982-0](#).
- [55] Y. Bai, Dark Matter is Darker, *NUCLEAR SCIENCE AND TECHNIQUES* 34 (6) (2023) 76. [doi:10.1007/s41365-023-01249-5](#).
- [56] L. Si, et al., Determination of Double Beta Decay Half-Life of ^{136}Xe with the PandaX-4T Natural Xenon Detector, *Research* 2022 (2022) 9798721. [arXiv:2205.12809](#), [doi:10.34133/2022/9798721](#).
- [57] X. Yan, et al., Searching for Two-Neutrino and Neutrinoless Double Beta Decay of ^{134}Xe with the PandaX-4T Experiment [arXiv:2312.15632](#).
- [58] S. Agostinelli, et al., GEANT4—a simulation toolkit, *Nucl. Instrum. Meth. A* 506 (2003) 250–303. [doi:10.1016/S0168-9002\(03\)01368-8](#).
- [59] M. Yeh, S. Hans, W. Beriguete, R. Rosero, L. Hu, R. L. Hahn, M. V. Diwan, D. E. Jaffe, S. H. Kettell, L. Littenberg, A new water-based liquid scintillator and potential applications, *Nucl. Instrum. Meth. A* 660 (2011) 51–56. [doi:10.1016/j.nima.2011.08.040](#).
- [60] T. Adam, et al., The OPERA experiment target tracker, *Nucl. Instrum. Meth. A* 577 (2007) 523–539. [arXiv:physics/0701153](#), [doi:10.1016/j.nima.2007.04.147](#).
- [61] P. Adamson, et al., The MINOS scintillator calorimeter system, *IEEE Trans. Nucl. Sci.* 49 (2002) 861–863. [doi:10.1109/TNS.2002.1039579](#).
- [62] F. Aharonian, et al., Performance test of the electromagnetic particle detectors for the LHAASO experiment, *Nucl. Instrum. Meth. A* 1001 (2021) 165193. [doi:10.1016/j.nima.2021.165193](#).

- [63] G. Luo, et al., Design optimization of plastic scintillators with wavelength-shifting fibers and silicon photomultiplier readouts in the top veto tracker of the JUNO-TAO experiment, Nucl. Sci. Tech. 34 (7) (2023) 99. [arXiv:2302.12669](#), [doi:10.1007/s41365-023-01263-7](#).
- [64] N. Ackerman, et al., The EXO-200 detector, part II: auxiliary systems, JINST 17 (02) (2022) P02015. [arXiv:2107.06007](#), [doi:10.1088/1748-0221/17/02/P02015](#).
- [65] C. Buck, B. Gramlich, S. Schoppmann, Novel Opaque Scintillator for Neutrino Detection, JINST 14 (11) (2019) P11007. [arXiv:1908.03334](#), [doi:10.1088/1748-0221/14/11/P11007](#).
- [66] E. Aprile, H. Contreras, L. W. Goetzke, A. J. Melgarejo Fernandez, M. Messina, J. Naganoma, G. Plante, A. Rizzo, P. Shagin, R. Wall, Measurements of proportional scintillation and electron multiplication in liquid xenon using thin wires, JINST 9 (11) (2014) P11012. [arXiv:1408.6206](#), [doi:10.1088/1748-0221/9/11/P11012](#).
- [67] T. Ye, K. L. Giboni, X. Ji, Initial evaluation of proportional scintillation in liquid Xenon for direct dark matter detection, JINST 9 (12) (2014) P12007. [doi:10.1088/1748-0221/9/12/P12007](#).
- [68] P. Juyal, K.-L. Giboni, X.-D. Ji, J.-L. Liu, On proportional scintillation in very large liquid xenon detectors, Nucl. Sci. Tech. 31 (9) (2020) 93. [arXiv:1910.13160](#), [doi:10.1007/s41365-020-00797-4](#).
- [69] A. Abusleme, et al., [Radioactivity control strategy for the juno detector](#), Journal of High Energy Physics 102. [doi:10.1007/JHEP11\(2021\)102](#).
URL [https://doi.org/10.1007/JHEP11\(2021\)102](https://doi.org/10.1007/JHEP11(2021)102)
- [70] C. Cao, N. Li, X. Yang, J. Zhao, Y. Li, Z. Cai, L. Wen, X. Luo, Y. Heng, Y. Ding, [A practical approach of high precision u and th concentration measurement in acrylic](#), Nuclear Instruments and Methods in Physics Research Section A: Accelerators, Spectrometers, Detectors and Associated Equipment 1004 (2021) 165377. [doi:https://doi.org/10.1016/j.nima.2021.165377](#).
URL <https://www.sciencedirect.com/science/article/pii/S0168900221003612>
- [71] E. Aprile, et al., Energy resolution and linearity of XENON1T in the MeV energy range, Eur. Phys. J. C 80 (8) (2020) 785. [arXiv:2003.03825](#), [doi:10.1140/epjc/s10052-020-8284-0](#).
- [72] L. Luo, et al., Improvement on the Linearity Response of PandaX-4T with new Photomultiplier Tubes Bases [arXiv:2401.00373](#).
- [73] K. Ozaki, S. Kazama, M. Yamashita, Y. Itow, S. Moriyama, Characterization of New Silicon Photomultipliers with Low Dark Noise at Low Temperature, JINST 16 (03) (2021) P03014. [arXiv:2007.13537](#), [doi:10.1088/1748-0221/16/03/P03014](#).
- [74] C. He, et al., [A 500 MS/s waveform digitizer for PandaX dark matter experiments](#), Journal of Instrumentation 16 (12) (2021) T12015. [doi:10.1088/1748-0221/16/12/t12015](#).
URL <https://doi.org/10.1088/1748-0221/16/12/t12015>
- [75] Y. Zhou, X. Chen, Data reduction strategy in the PandaX-4T experiment [arXiv:2311.12412](#).
- [76] X. Wang, Z. Lei, Y. Ju, J. Liu, N. Zhou, Y. Chen, Z. Wang, X. Cui, Y. Meng, L. Zhao, Design, construction and commissioning of the PandaX-30T liquid xenon management system, JINST 18 (05) (2023) P05028. [arXiv:2301.06044](#), [doi:10.1088/1748-0221/18/05/P05028](#).
- [77] H. Gong, K. L. Giboni, X. Ji, A. Tan, L. Zhao, The Cryogenic System for the Panda-X Dark Matter Search Experiment, JINST 8 (2013) P01002. [arXiv:1207.5100](#), [doi:10.1088/1748-0221/8/01/P01002](#).
- [78] L. Zhao, X. Cui, W. Ma, Y. Fan, K. Giboni, T. Zhang, J. Liu, X. Ji, The cryogenics and xenon handling system for the PandaX-4T experiment, JINST 16 (06) (2021) T06007. [arXiv:2012.10583](#), [doi:10.1088/1748-0221/16/06/T06007](#).
- [79] K. L. Giboni, P. Juyal, E. Aprile, Y. Zhang, J. Naganoma, A LN₂-based cooling system for a next-generation liquid xenon dark matter detector, Nucl. Sci. Tech. 31 (8) (2020) 76. [arXiv:1909.09698](#), [doi:10.1007/s41365-020-00786-7](#).
- [80] E. Aprile, et al., Search for New Physics in Electronic Recoil Data from XENONnT, Phys. Rev. Lett. 129 (16) (2022) 161805. [arXiv:2207.11330](#), [doi:10.1103/PhysRevLett.129.161805](#).
- [81] Z. Wang, et al., [Large scale xenon purification using cryogenic distillation for dark matter detectors](#), Journal of Instrumentation 9 (2014) P11024. [doi:10.1088/1748-0221/9/11/P11024](#).
URL <https://iopscience.iop.org/article/10.1088/1748-0221/9/11/P11024>
- [82] X. Cui, et al., [Design and commissioning of the pandax-4t cryogenic distillation system for krypton and radon removal](#), Journal of Instrumentation 16 (2021) P07046. [doi:10.1088/1748-0221/16/07/P07046](#).
URL <https://iopscience.iop.org/article/10.1088/1748-0221/16/07/P07046>
- [83] N. Abgrall, et al., The Majorana Demonstrator radioassay program, Nucl. Instrum. Meth. A 828 (2016) 22–36. [arXiv:1601.03779](#), [doi:10.1016/j.nima.2016.04.070](#).

- [84] J. B. Albert, et al., [Investigation of radioactivity-induced backgrounds in exo-200](#), Phys. Rev. C 92 (2015) 015503. doi:10.1103/PhysRevC.92.015503. URL <https://link.aps.org/doi/10.1103/PhysRevC.92.015503>
- [85] R. Agnese, et al., [Projected sensitivity of the supercdms snolab experiment](#), Phys. Rev. D 95 (2017) 082002. doi:10.1103/PhysRevD.95.082002. URL <https://link.aps.org/doi/10.1103/PhysRevD.95.082002>
- [86] E. Aprile, et al., [Double-Weak Decays of \$^{124}\text{Xe}\$ and \$^{136}\text{Xe}\$ in the XENON1T and XENONnT Experiments](#), Phys. Rev. C 106 (2) (2022) 024328. arXiv:2205.04158, doi:10.1103/PhysRevC.106.024328.
- [87] F. Agostini, et al., [Sensitivity of the DARWIN observatory to the neutrinoless double beta decay of \$^{136}\text{Xe}\$](#) , Eur. Phys. J. C 80 (9) (2020) 808. arXiv:2003.13407, doi:10.1140/epjc/s10052-020-8196-z.
- [88] Z. Guo, et al., [Muon flux measurement at China Jinping Underground Laboratory](#), Chin. Phys. C 45 (2) (2021) 025001. arXiv:2007.15925, doi:10.1088/1674-1137/abccae.
- [89] X. Chen, et al., [BambooMC — a Geant4 simulation program for the PandaX experiments](#), Journal of Instrumentation 16 (09) (2021) T09004. doi:10.1088/1748-0221/16/09/t09004. URL <http://dx.doi.org/10.1088/1748-0221/16/09/T09004>
- [90] Z. Qian, et al., [Low radioactive material screening and background control for the PandaX-4T experiment](#), Journal of High Energy Physics 147. doi:10.1007/JHEP06(2022)147. URL [https://doi.org/10.1007/JHEP06\(2022\)147](https://doi.org/10.1007/JHEP06(2022)147)
- [91] D. G. Madland, E. D. Arthur, G. P. Estes, J. E. Stewart, M. Bozoian, R. T. Perry, T. A. Parish, T. H. Brown, T. R. England, W. B. Wilson, W. S. Charlton, [Sources 4a: A code for calculating \(alpha,n\), spontaneous fission, and delayed neutron sources and spectradoi:10.2172/15215](#). URL <https://www.osti.gov/biblio/15215>
- [92] Q. Wang, et al., [An Improved Evaluation of the Neutron Background in the PandaX-II Experiment](#), Sci. China Phys. Mech. Astron. 63 (3) (2020) 231011. arXiv:1907.00545, doi:10.1007/s11433-019-9603-9.
- [93] M. Szydagis, N. Barry, K. Kazkaz, J. Mock, D. Stolp, M. Sweany, M. Tripathi, S. Uvarov, N. Walsh, M. Woods, [Nest: a comprehensive model for scintillation yield in liquid xenon](#), Journal of Instrumentation 6 (10) (2011) P10002. doi:10.1088/1748-0221/6/10/P10002. URL <https://dx.doi.org/10.1088/1748-0221/6/10/P10002>
- [94] D. Baxter, et al., [Recommended conventions for reporting results from direct dark matter searches](#), Eur. Phys. J. C 81 (10) (2021) 907. arXiv:2105.00599, doi:10.1140/epjc/s10052-021-09655-y.
- [95] E. A. Bagnaschi, et al., [Supersymmetric Dark Matter after LHC Run 1](#), Eur. Phys. J. C 75 (2015) 500. arXiv:1508.01173, doi:10.1140/epjc/s10052-015-3718-9.
- [96] W. Ma, et al., [Search for Solar B8 Neutrinos in the PandaX-4T Experiment Using Neutrino-Nucleus Coherent Scattering](#), Phys. Rev. Lett. 130 (2) (2023) 021802. arXiv:2207.04883, doi:10.1103/PhysRevLett.130.021802.
- [97] E. Bagnaschi, O. Buchmueller, R. Cavanaugh, M. Citron, A. De Roeck, M. Dolan, J. Ellis, H. Flächer, S. Heinemeyer, G. Isidori, et al., [Supersymmetric dark matter after lhc run 1](#), The European Physical Journal C 75 (10) (2015) 1–16.
- [98] E. Aprile, et al., [Dark Matter Search Results from a One Ton-Year Exposure of XENON1T](#), Phys. Rev. Lett. 121 (11) (2018) 111302. arXiv:1805.12562, doi:10.1103/PhysRevLett.121.111302.
- [99] D. S. Akerib, et al., [Results from a search for dark matter in the complete LUX exposure](#), Phys. Rev. Lett. 118 (2) (2017) 021303. arXiv:1608.07648, doi:10.1103/PhysRevLett.118.021303.
- [100] E. Aprile, et al., [Constraining the spin-dependent WIMP-nucleon cross sections with XENON1T](#), Phys. Rev. Lett. 122 (14) (2019) 141301. arXiv:1902.03234, doi:10.1103/PhysRevLett.122.141301.
- [101] D. S. Akerib, et al., [Limits on spin-dependent WIMP-nucleon cross section obtained from the complete LUX exposure](#), Phys. Rev. Lett. 118 (25) (2017) 251302. arXiv:1705.03380, doi:10.1103/PhysRevLett.118.251302.
- [102] M. J. Dolinski, A. W. P. Poon, W. Rodejohann, [Neutrinoless Double-Beta Decay: Status and Prospects](#), Ann. Rev. Nucl. Part. Sci. 69 (2019) 219–251. arXiv:1902.04097, doi:10.1146/annurev-nucl-101918-023407.
- [103] S. Kumaran, L. Ludhova, O. Penek, G. Settanta, [Borexino Results on Neutrinos from the Sun and Earth](#), Universe 7 (7) (2021) 231. arXiv:2105.13858, doi:10.3390/universe7070231.

- [104] B. Aharmim, S. Ahmed, A. Anthony, N. Barros, E. Beier, A. Bellerive, B. Beltran, M. Bergevin, S. Biller, K. Boudjemline, et al., Combined analysis of all three phases of solar neutrino data from the sudbury neutrino observatory, *Physical Review C* 88 (2) (2013) 025501.
- [105] N. Vinyoles, A. M. Serenelli, F. L. Villante, S. Basu, J. Bergström, M. Gonzalez-Garcia, M. Maltoni, C. Peña-Garay, N. Song, A new generation of standard solar models, *The Astrophysical Journal* 835 (2) (2017) 202.
- [106] M. Agostini, et al., Limiting neutrino magnetic moments with Borexino Phase-II solar neutrino data, *Phys. Rev. D* 96 (9) (2017) 091103. doi:10.1103/PhysRevD.96.091103.
- [107] A. Beda, V. Brudanin, V. Egorov, D. Medvedev, V. Pogosov, E. Shevchik, M. Shirchenko, A. Starostin, I. Zhitnikov, Gemma experiment: The results of neutrino magnetic moment search, *Phys. Part. Nucl. Lett.* 10 (2013) 139–143. doi:10.1134/S1547477113020027.
- [108] M. M. Miller Bertolami, Limits on the neutrino magnetic dipole moment from the luminosity function of hot white dwarfs, *Astron. Astrophys.* 562 (2014) A123. doi:10.1051/0004-6361/201322641.
- [109] S. A. Díaz, K.-P. Schröder, K. Zuber, D. Jack, E. E. B. Barrios, Constraint on the axion-electron coupling constant and the neutrino magnetic dipole moment by using the tip-RGB luminosity of fifty globular clusters [arXiv:1910.10568](https://arxiv.org/abs/1910.10568).
- [110] E. Aprile, et al., Excess electronic recoil events in XENON1T, *Phys. Rev. D* 102 (7) (2020) 072004. [arXiv:2006.09721](https://arxiv.org/abs/2006.09721), doi:10.1103/PhysRevD.102.072004.
- [111] A. Hitachi, T. Takahashi, N. Funayama, K. Masuda, J. Kikuchi, T. Doke, [Effect of ionization density on the time dependence of luminescence from liquid argon and xenon](https://arxiv.org/abs/1908.07279), *Phys. Rev. B* 27 (1983) 5279–5285. doi:10.1103/PhysRevB.27.5279. URL <https://link.aps.org/doi/10.1103/PhysRevB.27.5279>
- [112] J. P. Brodsky, S. Sangiorgio, M. Heffner, T. Stiegler, Background Discrimination for Neutrinoless Double Beta Decay in Liquid Xenon Using Cherenkov Light, *Nucl. Instrum. Meth. A* 922 (2019) 76–83. [arXiv:1812.05694](https://arxiv.org/abs/1812.05694), doi:10.1016/j.nima.2018.12.057.
- [113] M. Honda, M. Sajjad Athar, T. Kajita, K. Kasahara, S. Midorikawa, Atmospheric neutrino flux calculation using the NRLMSISE-00 atmospheric model, *Phys. Rev. D* 92 (2) (2015) 023004. [arXiv:1502.03916](https://arxiv.org/abs/1502.03916), doi:10.1103/PhysRevD.92.023004.
- [114] Y. Zhuang, L. E. Strigari, R. F. Lang, Time variation of the atmospheric neutrino flux at dark matter detectors, *Phys. Rev. D* 105 (4) (2022) 043001. [arXiv:2110.14723](https://arxiv.org/abs/2110.14723), doi:10.1103/PhysRevD.105.043001.
- [115] Y. Suzuki, Low-energy solar neutrino detection by using liquid xenon, in: *Workshop on Solar Neutrinos below 1-MeV: NuLow*, 2000. [arXiv:hep-ph/0008296](https://arxiv.org/abs/hep-ph/0008296), doi:10.1142/9789812778000_0009.